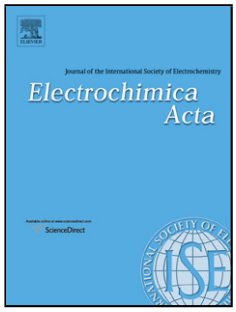

Title: Synthesis, electrochemical impedance spectroscopy study and photoelectrochemical behaviour of as-deposited and annealed WO_3 films

Author: R. Levinas N. Tsyntsaru M. Lelis H. Cesiulis

PII: S0013-4686(16)32671-8
DOI: http://dx.doi.org/doi:10.1016/j.electacta.2016.12.112
Reference: EA 28584

To appear in: *Electrochimica Acta*

Received date: 25-8-2016
Revised date: 13-12-2016
Accepted date: 19-12-2016

Please cite this article as: R.Levinas, N.Tsyntsaru, M.Lelis, H.Cesiulis, Synthesis, electrochemical impedance spectroscopy study and photoelectrochemical behaviour of as-deposited and annealed WO3 films, Electrochimica Acta http://dx.doi.org/10.1016/j.electacta.2016.12.112

Synthesis, electrochemical impedance spectroscopy study and photoelectrochemical behaviour of as-deposited and annealed WO_3 films

R. Levinas[1], N. Tsyntsaru[1,2,*,], M. Lelis[3], H. Cesiulis[1]**

[1]*Vilnius University, Naugarduko str. 24, Vilnius, Lithuania*

[2]*Institute of Applied Physics of ASM, Academiei str. 5, Chisinau, Republic of Moldova*

[3]*Lithuanian Energy Institute, Kaunas, Lithuania*

**Corresponding author: tintaru@phys.asm.md*

*** ISE member, ORCID ID* 0000-0002-9813-2460

Abstract

WO_3 films have been obtained by anodization of tungsten in the different acidic electrolytes (HCl, H_2SO_4, H_3PO_4, H_3PO_4 + NH_4F) and at various applied potentials. Electrochemical impedance spectroscopy was used to investigate film formation and to characterize the obtained oxide films. The equivalent electric circuits modelling reactive and blocking behaviour are provided and discussed. It was found, that oxide film capacitance decreases linearly with increasing anodization potential. The relative permittivity of tungsten oxide films varies from 31 to 56 depending on the acid used. A relatively high rate of the film formation (1.87 nm V^{-1}) and increased resistance against oxide breakdown can be achieved for tungsten oxide obtained from 0.3 M oxalic acid bath. Compact oxide films are formed at the potentials ranged from 10 V to 30 V, whereas increasing of anodization voltage to 60 V resulted in the formation of disordered, porous structures due to surface etching. Semiconductor properties were determined by Mott-Schottky analysis. Photoelectrochemical properties of as-deposited and annealed at 600°C WO_3 films were determined in a Na_2SO_4 solution under pulsed and constant UV irradiation. It was determined that annealed WO_3 films in comparison to as-deposited films are more stable and generate substantially higher photelectrochemical currents.

Keywords: anodization, tungsten trioxide, electrochemical impedance spectroscopy, annealing, photocurrent.

1. Introduction

Semiconductor materials have been always an area of particular interest. Most transition metal oxides exhibit semiconductor properties and are widely used in both industry and science. Currently, research on the rarer metal oxides (such as tungsten or molybdenum) remains important, especially in the increasingly vital solar energy conversion field. Anodization is a convenient and effective way to form an oxide film, because the anodic dissolution of metallic tungsten is followed by immediate formation of WO_3. One of the first models explaining the formation of WO_3 is the so-called Point Defect Model (PDM) [1-2]. It states that the formation of the oxide layer occurs via transfer of oxygen vacancies (point defects) from the metal | oxide interface, across the growing oxide layer, to the oxide | electrolyte interface, at which the vacancies are consumed. According to the PDM, the film thickness depends on the applied anodization potential. The interpretation of electrochemical impedance spectra in the frame of elaborated kinetic models or equivalent electric circuits is a powerful tool to investigate the formation mechanism of thin films [3-5].

The presence of a pseudo-inductive loop in the impedance spectra at intermediate frequencies indicates point defect interaction during the film growth and dissolution processes. A kinetic model, including the recombination reaction between positively and negatively charged point defects at the film/solution interface, as well as an elaborated kinetic scheme for tungsten diffusion through the film, mediated by cation vacancies, have been proposed. It is assumed that AC modulation of the space-charge layer within the oxide, and the compensating surface charge cause the relaxation phenomenon that results in inductance presence in the impedance spectrum [6].

The formation of a porous oxide layer occurs through equilibrium between electrochemical film formation and chemical dissolution. As the oxide dissolves, pits form on its surface and merge into porous structures [7]. Varieties of acidic media, as well as combinations with fluoride ions which dissolve tungsten via a different pathway, have been used for anodizing tungsten [8-13]. Oxide films obtained at different conditions (potential, pH, anodization duration and electrolyte used) exhibit different surface

morphology, thickness, and porosity. Thus, their photocatalytic properties can vary in a broad range [13, 14-18]. For commercial use, stable films are highly desirable. However, in many electrolytes WO_3 is susceptible to photocorrosion. A decrease of 74% in photocurrent density of electrodeposited films was noticed [19], after which the photocurrent remains constant for a long time. A significantly smaller drop of 39% was found for films, prepared via the polymeric precursor method [20] and 28.4% for vertically aligned plate-like arrays [21].

The stability of anodized WO_3 films can be further increased by thermal annealing [17-22]. This is likely caused by changes in crystallinity of the as-anodized films (from amorphous to monoclinic/orthorhombic). Temperatures above 400 ºC seem to decay surface porosity, but increase the overall thickness of the porous layer.

It was found that the photoelectrochemical properties of WO_3 films strongly depend on the film thickness. A decrease of measured optical band gap (from 2.96 eV to 2.50 eV) was observed for electrodeposited WO_3 films with thickness increase (respectively 168 nm to 431 nm) [23].

Further growth of film thickness (> 600) nm leads to a diminution in photocurrent conversion efficiency [24]. It was proposed that for films thinner than 500 nm the surface band gap component dominates. Whereas for thicker films (> 500 nm) it is the bulk band gap component that determines the photocurrent. Thicker films may also have increased resistivity, larger distance of charge carrier diffusion, and greater possibility of electron-hole pair recombination [25]. Multiple studies have shown that the limiting factor of the WO_3 film's photocatalytic properties is the generation of charge carriers by photons [26, 27]) and therefore a linear relation between illumination intensity and generated photocurrent was determined. The present study was devoted to the synthesis, electrochemical impedance spectroscopy (EIS) study and photoelectrochemical behaviour of as-deposited and annealed WO_3 films.

2. Experimental

All electrodes were prepared from pure W (99.95%, Alfa Aesar): (a) plates of 1 cm x 1 cm dimensions were used for structural analysis and photocurrent measurements; (b) wire of 1 cm^2 surface area was used

for voltammetry and electrochemical impedance spectroscopy. Prior to experiments, the electrodes were polished, degreased in acetone in the ultrasonic bath and rinsed with distilled water. Based on previous research [2, 3, 8-13], several electrolytes have been selected, and are presented in Table 1. All measurements were carried out using programmable potentiostat Autolab 302N and NOVA software. For high-voltage anodization, a Consort EV 245 galvanostat/potentiostat was used.

Table 1.

Tungsten oxidation at relatively low anodic potentials. Polarization curves were obtained by linear sweep voltammetry in the 0–5 V potential range at scan rate of 50 mV s^{-1}. A two-electrode cell with a stainless steel coil of significantly larger surface area (~30 cm^2) was used as counter electrode. It was considered that the possible potential shift during the measurement would be negligible compared to the applied voltage.

Electrochemical impedance spectra were registered as follows: an automated program has been set up to increase the potential in steps of 0.1 V (see Table 1). During each of these step, the electrode was kept at corresponding anodization potential for 10 minutes (a steady-state current has been settled within this period), then EIS spectrum was registered in the 10 kHz – 0.01 Hz frequency range at perturbation amplitude of ±5 mV. In this way, a continuous growth of the oxide film could be examined *in situ*. Measurements were conducted in a two-electrode cell. Due to the bigger electrode area and large capacitance of the counter electrode, the measured impedance belonged entirely to the working electrode.

The obtained EIS data quality and causality was confirmed by applying Kramers-Kronig procedure integrated into the NOVA software. The determined residuals were very small for the real part of the impedance (up to 0.8%), and their distribution appears to be random. Larger residuals occur on the imaginary part; their appearance coincides with the frequency range that exhibits inductance in the spectrum. Even so, only a few points are particular outliers, and generally the residuals are also within the vicinity of 1%. The sum of squares of the relative residuals reflects the compliance to Kramers-Kronig transforms, because the overall sums of residuals, χ^2 were ranged from 10^{-6} to 10^{-4} dependently of solution.

Mott-Schottky plots were calculated based on the EIS data obtained. For these experiments the impedance of the working electrode was measured at one frequency of 1 kHz (± 5 mV amplitude) and at anodic potentials from 1.2 V to 0.1 V. After measurement of each point, the oxide layer was regenerated for one minute at a constant potential 1÷ 5 V. The capacitance was calculated by fitting of the obtained results with a RC circuit. This given frequency (1 kHz) is within the range when the capacitance can be attributed to the barrier layer only. Moreover, this frequency was used to compare our results with other published data.

Tungsten oxidation at relatively high anodic potentials. WO_3 films were obtained by anodization in a two-electrode cell for 30 minutes at voltages ranged from 10 to 60 V in 0.3 M oxalic acid. Surface morphology was evaluated with Hitachi S-3400N scanning electron microscope. The thickness of obtained oxide films was measured based on cross-section images.

Photocurrents were measured in a three-electrode quartz cell, with a stainless steel counter electrode and a saturated Ag/AgCl reference electrode. A 0.5 M Na_2SO_4 electrolyte was selected. Measurements were carried out by means of Autolab Optical Bench system with a calibrated UV LED (365 nm) and light intensities up to 80 mW cm^{-2} connected to Autolab N3012 potentiostat. To compare as-deposited and annealed WO_3 films, samples were obtained by anodizing in 0.3 M oxalic acid at applied potential of 35 V for 30 minutes, then have been thermally treated for 3 hours at 600 ºC with a temperature ramp-up speed of 130-145 ºC min^{-1}.

3. Results and discussion

3.1 Tungsten oxidation at relatively low anodic potentials

In order to compare the formation of WO_3 in different electrolytes, potentiodynamic anodic curves for tungsten electrode were recorded in following solutions: 1 M H_2SO_4, 1M HCl, 14 M H_3PO_4, 14 M H_3PO_4 + 1 M NH_4F, and 0.3 M oxalic acid. Obtained anodic polarization curves for tungsten in various solutions are shown in Fig. 1. The shape of the curves is similar: a broad peak is followed by a wide passivation-dissolution plateau that extends at least up to 5 V. The peak is less pronounced in phosphoric acid with and without the addition of ammonium fluoride. In the presence of ammonium fluoride oxide dissolution

is somehow facilitated by the formation of fluoride complexes with W(VI), and peak current density increases slightly.

The polarization curves obtained in H_2SO_4 and HCl acids have similar shapes as in phosphoric acid solutions, but the peak current values are slightly larger. In the case of oxalic acid (Fig 1), the highest peak and plateau current densities are observed: j_{peak}=3.0 mA cm^{-2} and j_{pl}=1.3 mA cm^{-2}.

Fig. 1

3.1.1 Electrochemical impedance spectroscopy study

In order to reveal the different anodization behaviour of tungsten in the investigated electrolytes the electrochemical impedance spectroscopy was used. The EIS spectra and the equivalent electric circuits that best fit to the obtained spectra, are given in Fig. 2 and 3, respectively. The shapes of Nyquist and Bode plots differ, and represent either reactive (H_3PO_4 solutions) or blocking (HCl and $H_2C_2O_4$ solutions) systems in accordance with classification based on the impedance behaviour at the low frequencies and provided in [28]. For reactive systems, when frequency approaches 0, the impedance magnitude reaches a finite value [29]. Phase angle also approaches 0, showing that the current and potential are in phase. The system is then conductive to direct current. Such behaviour can be seen on the Bode plots (see Fig. 2 a and b) of impedance in phosphoric acid solutions. Blocking systems, however, completely prevent passing of direct current. It follows that when frequency approaches zero, imaginary part of impedance, Z_{im}, approaches -∞. Tungsten passivation in hydrochloric and oxalic acids reveals a strong capacitive response at the low frequencies (Fig. 2, c and d).

The impedance magnitudes decrease in the following order of acids: H_3PO_4 > H_3PO_4 + HF > HCl > $H_2C_2O_4$, as it can be predicted from the potentiodynamic curves. Notably, the shapes of the Nyquist and Bode plots depend on the chemical composition of the solution and anodization potential. The increase in impedance magnitude with increasing anodization potential in all studied cases can probably be explained by the increasing film thickness in these systems.

In addition, in the range of intermediate frequencies a pseudo-inductive response is visible in the studied potential range (at 1 V and higher) that can be ascribed to the relaxation phenomena at the oxide film /

solution interface [4]. The differences that arise between impedance spectra in the investigated solutions are caused by the specific kinetics of WO_3 formation in chemically dissimilar solutions. The anodization of tungsten oxide in aqueous electrolytes is a complicated reaction, but can be represented as:

$$W + 3H_2O \rightarrow WO_3 + 6H^+ + 6e^- \quad (1)$$

Then, partial dissolution of formed WO_3 occurs in acidic media [2]:

$$WO_3 + 2H^+ \rightarrow WO_2^{2+} + H_2O \quad (2)$$

The addition of NH_4F to the solution promotes three reactions, which can occur simultaneously: (i) tungsten oxide formation – Eq. (1); (ii) tungsten dissolution through the oxide [6], because of increased defectiveness of the outermost layer of the oxide – Eq. (3); and (iii) WO_3 dissolution – Eq. (4). The last two reactions result in the formation of tungsten and fluoride complexes:

$$W + nF^- \rightarrow \left[WF_n\right]^{(n-6)} + 6e^- \quad (3)$$

$$WO_3 + 6H^+ + nF^- \rightarrow \left[WF_n\right]^{(n-6)} + 3H_2O \quad (4)$$

When the mentioned reactions occur under AC perturbation of small amplitude, the H_3PO_4 and H_3PO_4+NH_4F systems behave as reactive at the low frequencies (Fig. 2 *a* and *b*), and impedance spectra fit well to the equivalent circuit shown in Fig. 3a. The constant phase element (CPE) in the equivalent electric circuits used to fit obtained spectra represents the imperfection of double layer capacitance. In general, the impedance of CPE is given by:

$$Z(\omega) = \frac{1}{Q}(j\omega)^{-n} \quad (5)$$

where Q is a constant, and $0<n<1$.

After adding NH_4F to the H_3PO_4 electrolyte (Fig. 2c) a substantial decrease (6 to 10 times) in the system impedance is obtained (see Fig. 2a and b). It is caused by the electrochemical dissolution of W leading to the formation of complexes in the solution according to the reaction (3). In addition, the value of coefficient *n* (see Eq. (5)) decreases from 1 to 0.92 probably due to increased defectiveness of the oxide film in the presence of F^--ions.

Fig. 2

Fig. 3

EIS spectra obtained in HCl and oxalic acid solutions (Fig. 2c and d) are of similar shape, and demonstrate blocking behaviour at the low frequencies. Probably, in these systems the concentration of WO_2^{2+} formed in the reaction (2) reaches the point of supersaturation and an extra oxide layer of $WO_3 \cdot 2H_2O$ is formed by the following reaction [30]:

$$WO_2^{2+} + 3H_2O \rightarrow WO_3 \cdot 2H_2O + 2H^+ \quad (6)$$

Therefore, the electric equivalent circuit used to fit these impedance spectra contains the additional RC element connected in series (Fig. 3b) which is marked as “R2” and “C0”, and fitting to this equivalent circuit is shown in Fig. 2 c and d.

Based on the impedance fitting results and taking into account the physical meaning of the elements of equivalent electric circuits, it is possible to estimate the thickness of oxide layers formed at relatively low anodization potentials. The capacitive behaviour can be related to the thickness and the dielectric properties of the oxide film. However, in order to be able to separate the barrier layer capacitance (C_1) from the pseudocapacitance (C_0) we needed to look into this phenomenon. A zone bordering the oxide | electrolyte interface (the space-charge zone) can either accumulate or deplete charge under effect of the AC signal. Then a compensating surface charge will build up from the electrolyte. It is evident that this process will alternate along with the AC phase. Hence, a time-dependent capacitor appears at the low frequency range.

The values of equivalent electric circuit elements depending on the potential are shown in Fig. 4. With formation potential increasing, the oxide become thicker and both the capacitance of the barrier layer (C_1) and pseudocapacitance (C_0) decreases. Simultaneously, the charge transfer resistance (R_3) increases linearly because the charge carriers have to migrate a larger distance; the increase in resistance of the space charge layer (R_4) and in inductivity (L) can also be attributed to the larger film thickness.

Fig. 4

It has been proposed that the compact oxide layer could be modelled as a parallel plate capacitor, thus the capacitance of the barrier film should be inversely proportional to the distance between the plates, or in this case to the thickness of the film [3,5]:

$$C_1 = \frac{\varepsilon_r \varepsilon_0}{L} \tag{7}$$

where ε_r and ε_0 is the apparent relative permitivity of the oxide film and the permittivity of vacuum, respectively; L is the thickenss of obtained oxide film.

On the other hand, the thickness increases with applied potential (E_F) proportionally to a coefficient α, which is also called the anodizing or formation ratio. Hence, the thickness can be expressed by a linear equation:

$$L = \alpha\left(E_F - E_0\right) \tag{8}$$

where α is the anodizing ratio; E_F is the applied formation potential; E_0 is the starting potential of the oxide film formation.

Combining these two equations results in a linear dependence of the inverse capacitance on the film formation potential, and slope of this dependence is equal to $\frac{\alpha}{\varepsilon_r \varepsilon_0}$:

$$\frac{1}{C_1} = \frac{\alpha}{\varepsilon_r \varepsilon_0}\left(E_F - E_0\right) \tag{9}$$

It was found that tungsten oxide layer capacitance is represented by the CPE (see. Fig. 3 and 4), and the capacitance values were recalculated into effective capacitances, C_b, using the following equation [31]:

$$C_b = Q^{\frac{1}{n}} R_f^{\frac{1-n}{n}} \tag{10}$$

where R_f is the oxide layer resistance; Q and n are defined in Eq. 5.

The plots of the inverse capacitance on the applied potential for all investigated electrolytes are shown in Fig. 5.

Fig. 5

They are linear as it is predicted by Eq. 9, but slopes depend on the electrolyte used. The slope is higher in the case of HCl, H_2SO_4 and oxalic acid, than for phosphoric acid solutions. If the relative permittivity is assumed to be constant for the entire range of the applied potentials 1÷5 V, then according to Eq. 7 the capacitance decreases due to thickness increase. However, the estimation of film thickness from capacitance measurements is not straightforward. Most of the researchers are finding the constant of relative permittivity or are using other independent methods for thickness estimation. In this study the method reported in [3] was applied, and the indicated averaged value of the anodization ratio α=1.78 nm V^{-1} was used for calculations using Eq. 9. The calculated constants of relative permittivity are presented in Table 2 and estimated thickness of oxide layers vs anodization potential is shown in Fig. 6. Obviously, using of α as an average value results in some smoothing out of the results, although the differences between thickness of films formed in phosphoric acid and other electrolytes are seen clearly.

Table 2.

Fig. 6

3.1.2 Semiconductor properties of obtained WO_3 films

Semiconductor properties have been determined for tungsten oxide films obtained in 0.3 M oxalic acid using Mott-Schottky equation:

$$\frac{1}{C_{SC}^2} = \left(\frac{2}{q\varepsilon_r\varepsilon_0 N_D}\right)\left((V_F - V_{FB}) - \frac{kT}{q}\right) \quad (11)$$

where C_{SC} is the space-charge layer capacitance*;* q is the elementary charge; N_D is the donor density*;* V_F and V_{FB} are the oxide film formation potential and flat band potential, respectively.

In our case C_{SC} is equivalent to C_1 (Fig. 3). The Mott-Schottky plots shown in Fig. 7 were plotted based on the electrochemical impedance data obtained at the decreasing potential values from 1.2 V to 0.1 V.

After measurement of each point, the oxide layer was regenerated for one minute at a constant potential of 1 V to 5 V. The capacitance was calculated through fitting with a typical RC circuit, because at 1 kHz neither pseudocapacitance nor inductance should distort the fitting data.

The shape of plots reveals, that the obtained WO_3 is an n-type semiconductor. The interception of the trend lines with the ordinate gives the value of the flat band potential, while the donor density can be calculated from the slope of the plots. The results of these calculations are presented in Table 3, and show that both donor density and flat band potential vary with anodization potential. The drop in donor density can be related to the increase in film thickness; and the bulk donor concentration must decrease with increase in oxide volume. With rising formation potential from 2 V to 5 V the flat band potential shifts from 0.179 V to 0.371 V vs Ag/AgCl. Clearly, a change occurs in the oxide band structure, which may have an effect on its photoelectrochemical properties.

Fig. 7 - updated

Table 3

3.2 Tungsten oxidation at relatively high anodic potentials

High anodization potentials have been applied in order to obtain thicker tungsten oxide films, which are more suitable for photoelectrochemical behaviour study. Due to limited rate of tungsten oxide growth in phosphoric solutions (Fig. 6), only sulphuric, hydrochloric and oxalic acids have been used for anodization at the high potentials. Stationary polarization curves of tungsten anodization in investigated acidic solutions are shown in Fig. 8. The relatively high anodization potentials up to 70 V without film breakdown can be applied only in the oxalic acid, while the oxide layers obtained in 1 M H_2SO_4 and 1 M HCl solutions are not stable already at ~50 V. Also, the anodization current densities are much lower in these solutions than in oxalic acid.

Fig. 8

Therefore, only WO_3 films obtained in oxalic acid have been further investigated. SEM images of these films obtained at relatively high anodization potentials are shown in Fig. 9. It was observed that at

formation potential of 10-20 V a compact oxide film is obtained, which covers the entire surface uniformly. At formation potentials of 30 - 40 V, due to partial surface etching, nanoporous structures on the compact oxide layer are formed. However, the coverage of ordered nanoporous layer was not uniform (Fig. 9, inset images). At anodization potential of 60 V almost the entire surface of oxide film was affected by etching (Fig. 9).

Fig. 9

The thicknesses of the anodized films obtained at high anodization potentials were estimated from SEM images of the film cross-sections (Fig. 10, scatter points). The linear correlation between anodization potential and the resulted film thickness is observed. Based on these experimental data the anodization ratio α=1.87 nm V^{-1} was determined in the oxalic acid solution. This value was introduced into Eq. 8 to calculate the trend-line that was extended to the lower potentials as well (Fig. 10 solid line).

Fig. 10

The obtained value for anodization ratio is slightly higher than reported in [3] α=1.78 nm V^{-1}, which was determined as an average value for several electrolytes, and can result in underestimation of oxide film thickness. Thus, the comparison of the trend-lines, obtained by extrapolation of the data presented in Fig. 6 for oxalic acid (Fig. 10, dashed line) and experimental data (Fig. 10 solid line), reveals the difference in the estimation of the film thickness. Moreover, based on experimentally determined value of α, the relative permittivity for tungsten oxide obtained from oxalic acid solution has been updated from 31. 6 to 33.3 (Table 2).

3.3 Photoelectrochemical properties of as-deposited and annealed WO_3 films

It has been reported [14] that the band gap of WO_3 lies within the range of 2.6 eV to 3.0 eV, therefore the strongest light absorbance shall occur in the ultraviolet range. Photoelectrochemical properties of obtained tungsten oxide films in 0.3 M oxalic acid were investigated. Fig. 11 shows linear sweep voltammetry curves obtained in the presence and without UV irradiation in a Na_2SO_4 solution for as-anodized sample. There is a small peak at ~ -0.2 V, and its position and height do not depend on the UV irradiation intensity. It can likely be related to the oxidation of some remaining un-oxidized tungsten

through the formed oxide film. An increase in photocurrent is observed at potentials >1 V, where the photoelectrochemical splitting of water begins to occur. Further increasing of potential yields progressively stronger photocurrents. The increase of UV irradiation intensity also linearly increases the photocurrent density at any given potential.

Fig. 11. - updated

Chronoamperometric measurements under pulsed UV irradiation with 2 second on-off intervals have also been carried out on the obtained oxide films, and data are presented in Fig. 12. The highest photocurrent density (0.11 mA cm^{-2}) was observed for the film anodized at 80 V. According to the previously discussed results, this film would be the thickest and has the highest specific surface area. Although, some discrepancy can be seen at lower voltages, where changes in the surface structure might have had an effect, generally the bigger anodization voltage the larger is the photocurrent.

Although, the stability of WO_3 layers has not been a major task of this study, the film degradation was noticed. Namely, a change in film colour was detected during prolonged measurements and some films even can dissolve. Furthermore, after 200 seconds the photocurrent decreased by 10 – 20 μA cm^{-2} in most cases. In order to overcome the film stability issue, the annealing was performed as it increases the amount of oxygen vacancies and thus free electrons in the oxide, as well as improves the crystallinity [17]. The effects of annealing have been discussed in [12, 17], where it was found that the indirect band gap of WO_3 decreases almost linearly when annealing temperature increases from 300 ºC to 500 ºC. Consequently the photoelectrochemical properties of oxides improves [19].

Fig.12

Annealing of the WO_3 films obtained at potential of 35 V for 30 minutes was carried out for 3 hours at 600 ºC and the temperature ramp-up speed of 130-145 ºC min^{-1}. The measured photocurrents of these films are presented in Fig. 13. Annealed films showed faster response to UV illumination and higher photocurrents (up to 1 mA cm^{-2}) compared to as-deposited films generating photocurrent of ~0.11 mA cm^{-2}.

Fig. 13

The films also exhibit higher resistance to photocorrosion, because no decrease of photocurrent during the measurement was observed. Results of voltammetric measurements (Fig. 14) reveal that the photocurrent onset potential shifts to the lower anodic values after annealing due to possible changes in crystal structure. Also, an increase in photocurrent from 0.37 mA cm^{-2} at 0.5 V to 1.95 mA cm^{-2} at 2.4 V is observed. Thus, irradiation of annealed WO_3 films at higher potentials could result in enhanced photocatalytic behaviour for water splitting.

Fig. 14 - updated

4. Conclusions

The comprehensive investigation of as-deposited and annealed WO_3 films obtained by tungsten anodization in the different acidic solutions (1 M H_2SO_4, 1 M HCl, 14 M H_3PO_4, 14 M H_3PO_4 + 1 M NH_4F, 0.3 M oxalic acid) was carried out. Highest anodization currents of tungsten oxide formation were obtained for 0.3 M oxalic acid solution. The anodization behaviour of tungsten in the investigated electrolytes was studied by the electrochemical impedance spectroscopy. Electrochemical impedance magnitudes at the low frequency range decrease in the following order: H_3PO_4 > H_3PO_4 + HF > HCl > $H_2C_2O_4$. The lowest charge transfer resistances are obtained for oxalic acid that is in conformity with voltammetric data.

In addition, in the range of intermediate frequencies a pseudo-inductive response is visible, that can be ascribed to the relaxation phenomena at the oxide film / solution interface. The shapes of the Nyquist and Bode plots depend on the chemical composition of the solution and the anodization potential. Blocking (HCl and $H_2C_2O_4$) or reactive (H_3PO_4) behaviour was revealed based on EIS study. Also, Mott-Schottky analysis has been performed in order to evaluate semiconductor properties of the obtained films and was shown that both donor density and flat band potential vary with anodization potential.

A compact oxide film deposits at lower anodization potentials (<20 V), and some irregular, porous structures are formed at higher anodization potentials. The thickness of WO_3 formed in 0.3 M oxalic acid linearly depends on the anodization potential, and could reach 120 nm obtained at 60 V. The anodization ratio α = 1.87 nm V^{-1} and relative permittivity equal to 33.3 were determined for oxalic acid electrolyte.

Photoelectrochemical behaviour of as-deposited and annealed WO_3 films has been evaluated. The highest photocurrents were generated by films obtained at higher anodizing potentials (60 V – 80 V). Annealing at 600 ºC significantly improves the stability of oxide layer and increases the photocurrent. Thus, annealed WO_3 films manifest performed photocatalytic behaviour for water splitting in comparison to as-deposited.

Acknowledgments. This work was supported by Research Council of Lithuania (MIP-031/2014), Moldavian national project 15.817.02.05A.

References

[1] D.D. Macdonald, Steady-State Passive Films, J. Electrochem. Soc. 139 (1992) 170. doi:10.1149/1.2069165.

[2] D.D. Macdonald, The kinetics of growth of the passive film on tungsten in acidic phosphate solutions, Electrochim. Acta. 43 (1998) 2851–2861. doi:10.1016/S0013-4686(98)00026-7.

[3] S. Biaggio, R. Rocha-Filho, J. Vilche, A study of thin anodic WO_3 films by electrochemical impedance spectroscopy, Electrochim. Acta. 42 (1997) 1751–1758.

[4] M. Bojinov, The ability of a surface charge approach to describe barrier film growth on tungsten in acidic solutions, Electrochim. Acta. 42 (1997) 3489–3498. doi:10.1016/S0013-4686(97)00037-6.

[5] M. Metikoš-Huković, Z. Grubač, The growth kinetics of thin anodic WO_3 films investigated by electrochemical impedance spectroscopy, J. Electroanal. Chem. 556 (2003) 167–178. doi:10.1016/S0022-0728(03)00342-5.

[6] V. Karastoyanov, M. Bojinov, Anodic oxidation of tungsten in sulphuric acid solution-Influence of hydrofluoric acid addition, Mater. Chem. Phys. 112 (2008) 702–710. doi:10.1016/j.matchemphys.2008.06.029.

[7] N.R. De Tacconi, C.R. Chenthamarakshan, G. Yogeeswaran, A. Watcharenwong, R.S. De Zoysa, N.A. Basit, K. Rajeshwar, Nanoporous TiO_2 and WO_3 films by anodization of titanium and

tungsten substrates: Influence of process variables on morphology and photoelectrochemical response, J. Phys. Chem. B. 110 (2006) 25347–25355. doi:10.1021/jp064527v.

[8] S. Berger, H. Tsuchiya, A. Ghicov, P. Schmuki, High photocurrent conversion efficiency in self-organized porous WO_3, Appl. Phys. Lett. 88 (2006) 203119. doi:10.1063/1.2206696.

[9] M. Yang, N.K. Shrestha, P. Schmuki, Thick porous tungsten trioxide films by anodization of tungsten in fluoride containing phosphoric acid electrolyte, Electrochem. Commun. 11 (2009) 1908–1911. doi:10.1016/j.elecom.2009.08.014.S.

[10] S. Ismail, K.A. Razak, P.W. Jing, Z. Lockman, Tungsten oxide nanoporous structure synthesized via direct electrochemical anodization, AIP Conf. Proc. 1341 (2011) 21–24. doi:10.1063/1.3586946.

[11] N. Mukherjee, M. Paulose, O.K. Varghese, G.K. Mor, C. a. Grimes, Fabrication of nanoporous tungsten oxide by galvanostatic anodization, J. Mater. Res. 18 (2003) 2296–2299. doi:10.1557/JMR.2003.0321.

[12] T. Zhu, M.N. Chong, E.S. Chan, Nanostructured tungsten trioxide thin films synthesized for photoelectrocatalytic water oxidation: A review, Chem. Sus. Chem. 7 (2014) 2974–2997. doi:10.1002/cssc.201402089.

[13] Y. Liu, Y. Li, W. Li, S. Han, C. Liu, Photoelectrochemical properties and photocatalytic activity of nitrogen-doped nanoporous WO_3 photoelectrodes under visible light, Appl. Surf. Sci. 258 (2012) 5038–5045. doi:10.1016/j.apsusc.2012.01.080.

[14] R.M. Fernández-Domene, R. Sánchez-Tovar, B. Lucas-Granados, J. García-Antón, Improvement in photocatalytic activity of stable WO_3 nanoplatelet globular clusters arranged in a tree-like fashion: Influence of rotation velocity during anodization, Appl. Catal. B Environ. 189 (2016) 266–282. doi:10.1016/j.apcatb.2016.02.065.

[15] F. Di Quarto, A. Di Paola, C. Sunseri, Semiconducting properties of anodic WO3 amorphous films, Electrochim. Acta. 26 (1981) 1177–1184. doi:10.1016/0013.

[16] S. Caramori, V. Cristino, L. Meda, A. Tacca, R. Argazzi, C.A. Bignozzi, Efficient anodically grown WO_3 for photoelectrochemical water splitting, Energy Procedia. 22 (2011) 127–136. doi:10.1016/j.egypro.2012.05.214.

[17] Y. Chai, C.W. Tam, K.P. Beh, F.K. Yam, Z. Hassan, Effects of thermal treatment on the anodic growth of tungsten oxide films, Thin Solid Films. 588 (2015) 44–49. doi:10.1016/j.tsf.2015.04.033.

[18] S. Ismail, C. Ng, E. Ahmadi, K. Razak, Segmented nanoporous WO_3 prepared via anodization and their photocatalytic properties, J. Mater. Res. (2016). doi:10.1557/jmr.2016.71.

[19] M. Yagi, S. Maruyama, K. Sone, K. Nagai, T. Norimatsu, Preparation and photoelectrocatalytic activity of a nano-structured WO_3 platelet film, J. Solid State Chem. 181 (2008) 175–182. doi:10.1016/j.jssc.2007.11.018.

[20] W. Li, J. Li, X. Wang, J. Ma, Q. Chen, Photoelectrochemical and physical properties of WO_3 films obtained by the polymeric precursor method, Int. J. Hydrogen Energy. 35 (2010) 13137–13145. doi:10.1016/j.ijhydene.2010.09.011.

[21] J. Yang, W. Li, J. Li, D. Sun, Q. Chen, Hydrothermal synthesis and photoelectrochemical properties of vertically aligned tungsten trioxide (hydrate) plate-like arrays fabricated directly on FTO substrates, J. Mater. Chem. 22 (2012) 17744. doi:10.1039/c2jm33199c.

[22] C.Y. Ng, K. Abdul Razak, Z. Lockman, Effect of annealing temperature on anodized nanoporous WO_3, J. Porous Mater. 22 (2015) 537–544. doi:10.1007/s10934-015-9924-x.

[23] W.L. Kwong, H. Qiu, A. Nakaruk, P. Koshy, C.C. Sorrell, Photoelectrochemical properties of WO_3 thin films prepared by electrodeposition, Energy Procedia. 34 (2013) 617–626. doi:10.1016/j.egypro.2013.06.793.

[24] W.L. Kwong, N. Savvides, C.C. Sorrell, Electrodeposited nanostructured WO_3 thin films for photoelectrochemical applications, Electrochim. Acta. 75 (2012) 371–380. doi:10.1016/j.electacta.2012.05.019.

[25] B. Yang, P.R.F. Barnes, W. Bertram, V. Luca, Strong photoresponse of nanostructured tungsten trioxide films prepared via a sol-gel route, J. Mater. Chem. 17 (2007) 2722. doi:10.1039/b702097j.

[26] H. Wang, T. Lindgren, J. He, A. Hagfeldt, S.-E. Lindquist, Photolelectrochemistry of Nanostructured WO_3 Thin Film Electrodes for Water Oxidation: Mechanism of Electron Transport, J. Phys. Chem. B. 104 (2000) 5686–5696. doi:10.1021/jp0002751.

[27] N. Naseri, S. Yousefzadeh, E. Daryaei, A.Z. Moshfegh, Photoresponse and H_2 production of topographically controlled PEG assisted sol-gel WO_3 nanocrystalline thin films, Int. J. Hydrogen Energy. 36 (2011) 13461–13472. doi:10.1016/j.ijhydene.2011.07.129.

[28] M. E. Orazem, B. Tribollet, Electrochemical Impedance Spectroscopy (Wiley, New York, 2008), 523 pp

[29] M. E. Orazem, N. Pebere, B. Tribollet, Enhanced graphical representation of electrochemical impedance data, J. Electrochem. Soc. 153 (2006) B129—B136. doi: 10.1149/1.2168377

[30] C. Ng, C. Ye, Y.H. Ng, R. Amal, Flower-shaped tungsten oxide with inorganic fullerene-like structure: synthesis and characterization, Cryst. Growth Des. 10 (2010) 3794–3801.

[31] B. Hirschorn, M. E. Orazem, B. Tribollet, V. Vivier, I. Frateur, M. Musiani, Determination of effective capacitance and film thickness from constant-phase-element parameters, Electrochim Acta. 55 (2010) 6218—6227. doi: 10.1016/j.electacta.2009.10.065

Table 1. **Electrolytes and conditions of the EIS study.**

Electrolyte	Anodization potential range	No. of steps	Duration of each step
1 M HCl	0.1 V – 5.0 V	50	10 min.
1 M H_2SO_4			
14 M H_3PO_4			
14 M H_3PO_4 + 1 M NH_4F			
0.3 M oxalic acid			

Table 2. Values of relative permittivity (ε_r) of WO_3 films in the investigated solutions

Solution	ε_r
HCl	37.9
H_2SO_4	31.2
0.3 M oxalic acid	31.6; (33.3)*
14 M H_3PO_4	55.9

*Value is calculated based on the experimentally obtained α=1.87 nm V^{-1}

Table 3. Data of Mott-Schottky analysis.

E_F, V	V_{FB} vs. Ag/AgCl, V	N_D, cm^{-3}
2	0.179	$3.9\ 10^{20}$
3	0.260	$2.4\ 10^{20}$
4	0.302	$1.6\ 10^{20}$
5	0.371	$1.1\ 10^{20}$

Figure captions

Fig. 1. Potentiodynamic curves for tungsten anodization in the investigated solutions; potential scan rate 50 mV s^{-1}.

Fig. 2. Nyquist and Bode plots obtained for tungsten anodization at various potentials (indicated on the top) in the electrolytes: 14 M H_3PO_4 (a); 14 M H_3PO_4 + 1 M NH_4F (b); 1 M HCl (c); 0.3 M oxalic acid (d). Points are experimental data and solid lines are fitting results to the equivalent circuits (Fig. 3).

Fig. 3. Equivalent electrical circuits used to fit data shown in Fig. 2. (a): R_1 is the electrolyte resistance; CPE_1 is a constant phase element and ascribed to oxide layer capacitance; R_2 is the charge transfer resistance; R_3 is ascribed to resistance of the space-charge zone. L_1 is the inductance. (b): R_1 is the electrolyte resistance; C_0 is pseudo-capacitance; R_2 is the resistance of the pseudo-capacitor; CPE_1 is ascribed to oxide layer capacitance; R_3 is a charge transfer resistance; R_4 is the resistance of the space-charge zone; L_1 is the inductance.

Fig. 4. The values of the elements of equivalent electric circuit describing tungsten anodization in 0.3M oxalic acid as a function of anodizing potential. (a) C_0 and C_1 vs E; (b) n vs E; (c) L vs E.

Fig. 5. The dependence of the inverse oxide layer capacity on the formation potential.

Fig. 6 The thickness of oxide films vs anodization potential in the investigated solutions.

Fig. 7. ***Mott-Schottky plots for tungsten oxide films obtained in 0.3 M oxalic acid at various potentials.***

Fig. 8. Film thickness as a function of anodizing potential in 0.3 M oxalic acid solution. Points are experimental data; solid line is calculated using α=1.87 nm V^{-1}; and dashed line is calculated based on the data shown in Fig. 6.

Fig. 9. Anodic polarization curve of tungsten in 0.3 M oxalic acid, 1 M HCl, and 1 M H_2SO_4.

Fig. 10. SEM images of WO_3 films, obtained by 30 minutes anodization of tungsten in 0.3 M oxalic acid solution.

Fig. 11. Photocurrents of WO_3 obtained by anodizing for 30 minutes at 30 V in a 0.3 M oxalic acid solution. Photocurrents were measured in 0.5 M Na_2SO_4. Potential sweep rate 50 mV s^{-1}.

Fig. 12. Photocurrents of WO_3 films, obtained in 0.3 M oxalic acid for 30 min at different formation potentials. UV intensity is 80 mW cm^{-2}. Measured in 0.5 M Na_2SO_4 at 1 V anodic potential.

Fig. 13. Photocurrent of annealed WO_3 film measured in 0.5 M Na_2SO_4 at 1 V anodic potential; UV intensity is 80 mW cm^{-2}; on-off interval is10 s.

Fig. 14. Polarization curve of annealed WO_3 under pulsed UV irradiation obtained in 0.5 M Na_2SO_4; UV intensity is 80 mW cm^{-2}; on-off interval is 10 s; potential sweep rate – 10 mV s^{-1}.

Figure 1

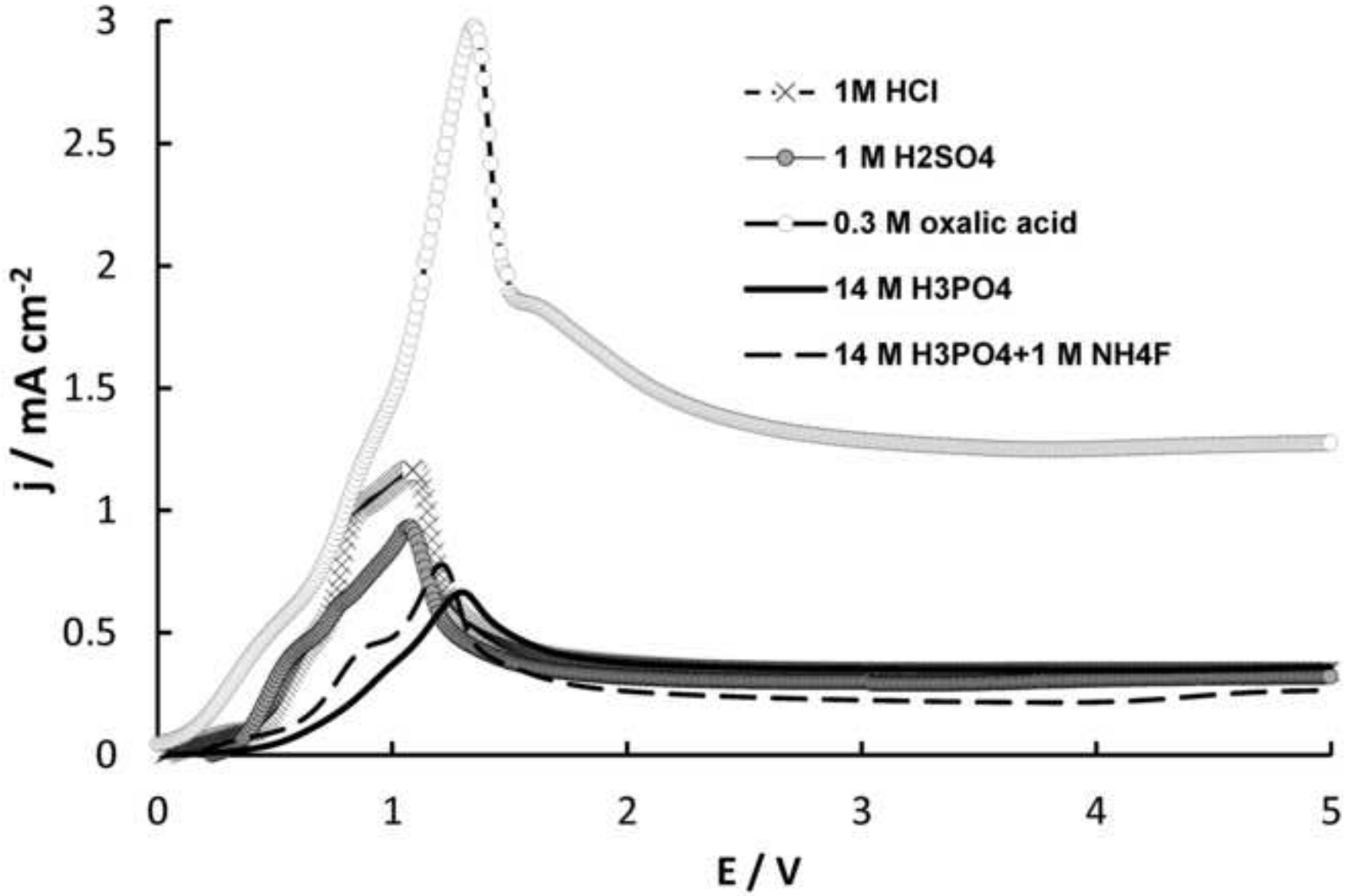
3
2.5
2
1.5
1
0.5
0
j / mA cm-2
0
1
2
3
4
5
E / V
1M HCl
1 M H2SO4
0.3 M oxalic acid
14 M H3PO4
14 M H3PO4+1 M NH4F

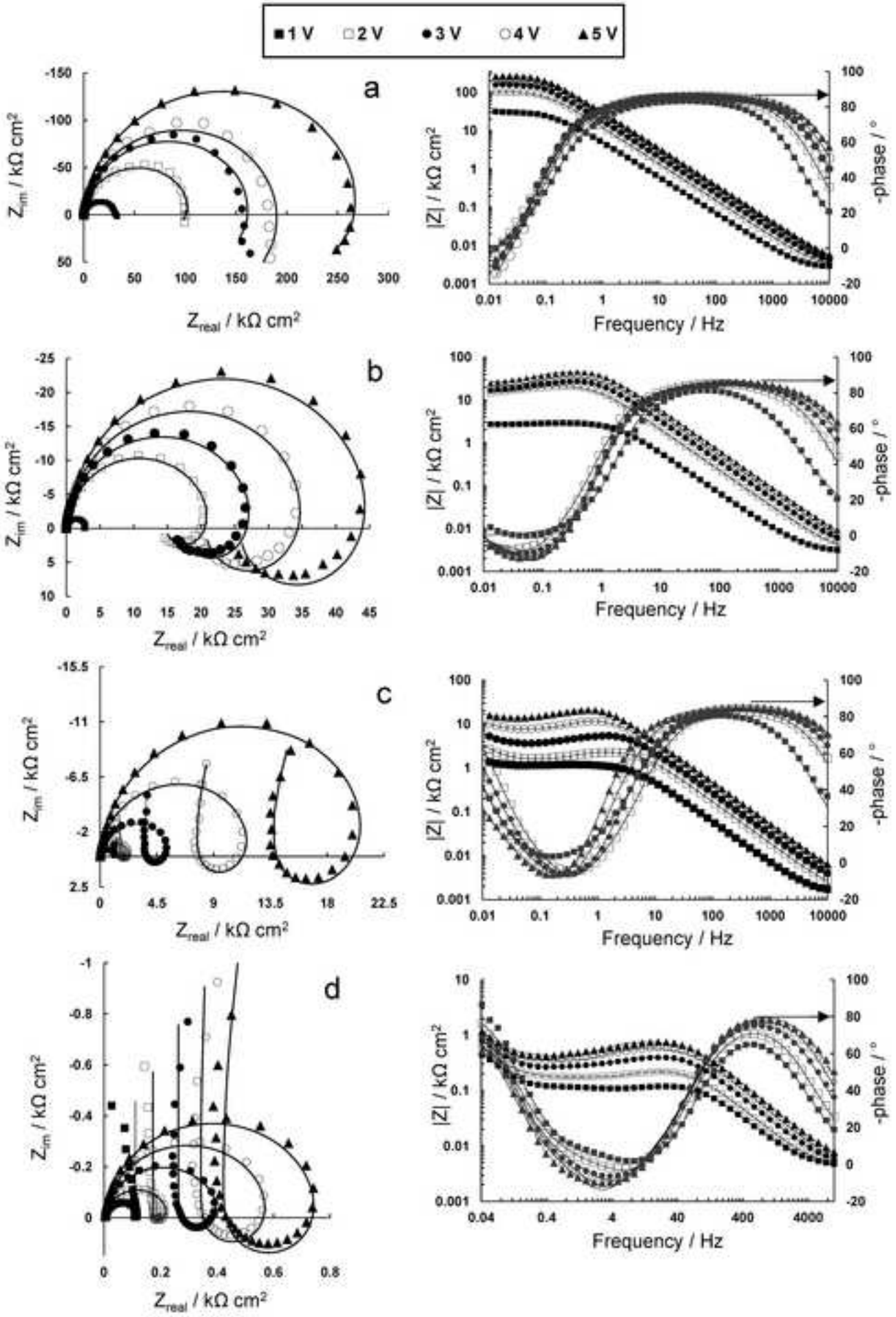

Figure 3

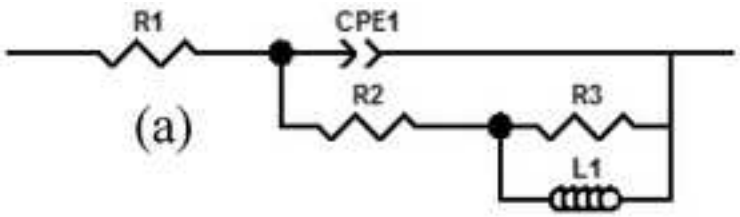

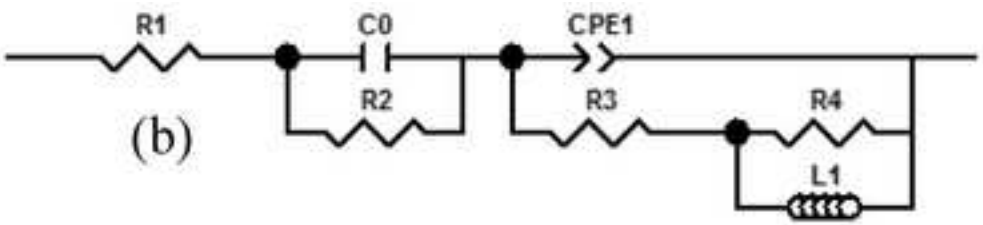

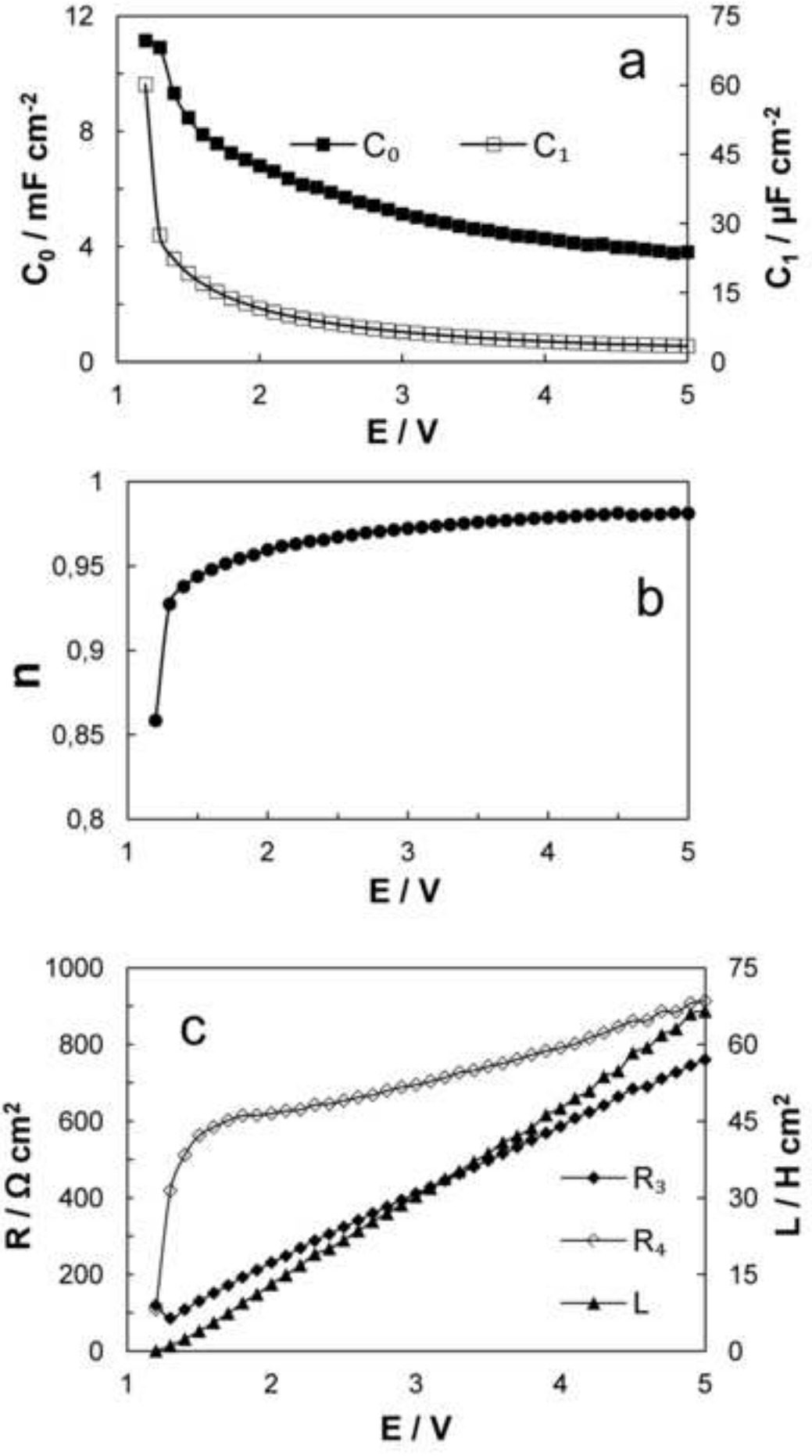

Figure 5

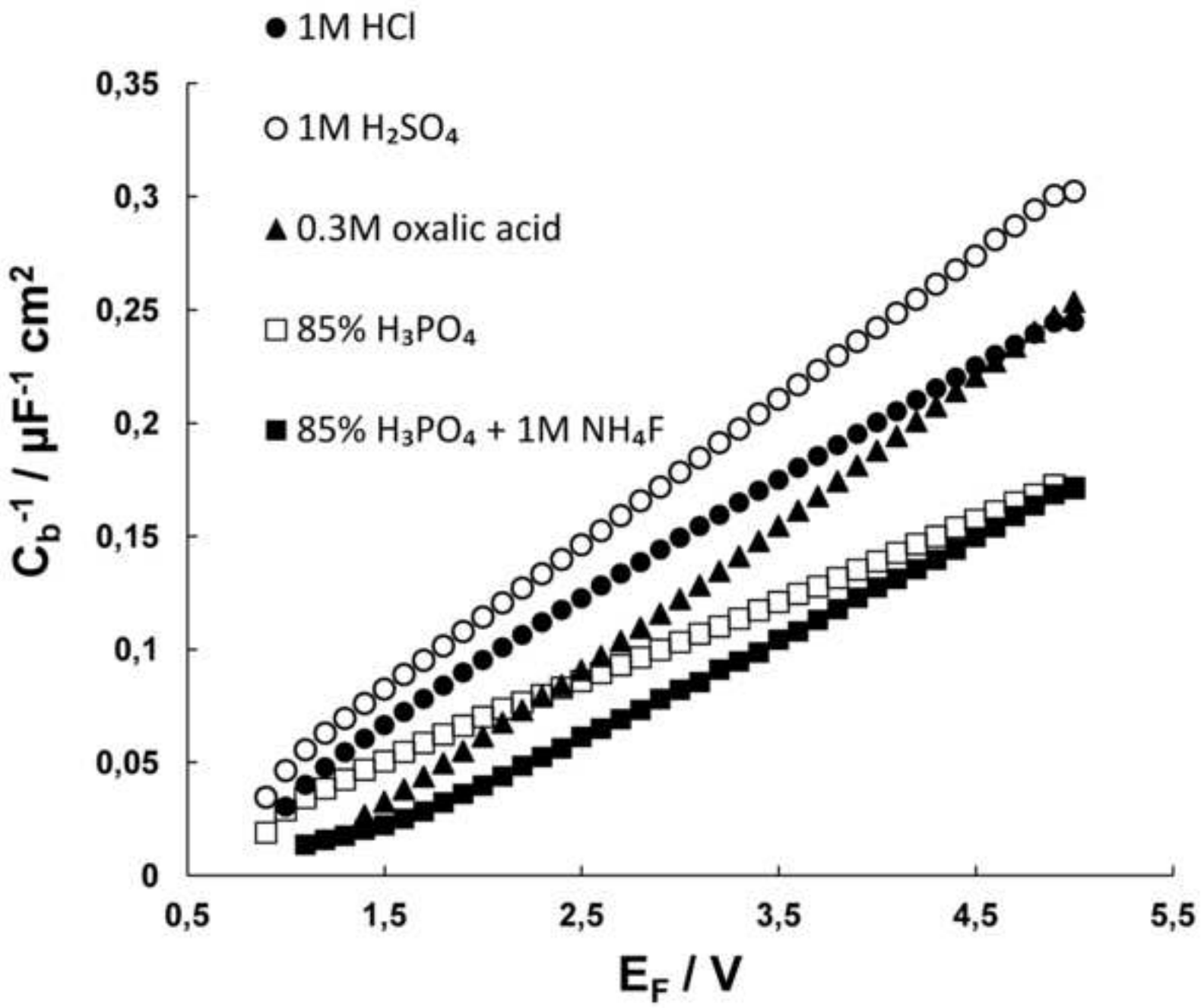
1M HCl
1M H2SO4
0.3M oxalic acid
85% H3PO4
85% H3PO4 + 1M NH4F
Cb-1 / µF-1 cm2
0,35
0,3
0,25
0,2
0,15
0,1
0,05
0
0,5
1,5
2,5
3,5
4,5
5,5
EF / V

Figure 6

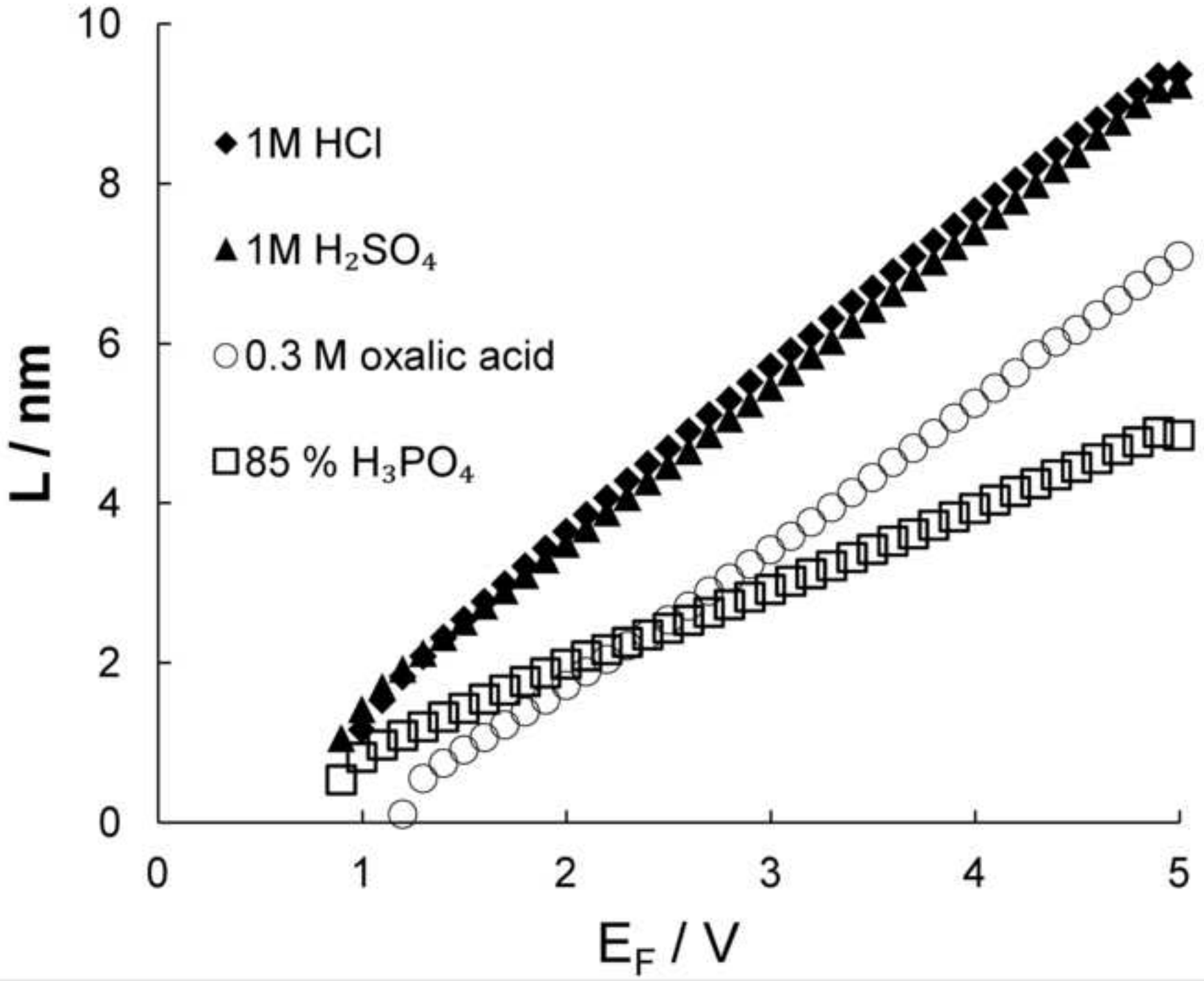
10
8
6
4
2
0
L / nm
1M HCl
1M H2SO4
0.3 M oxalic acid
85 % H3PO4
0
1
2
3
4
5
EF / V

Figure 7

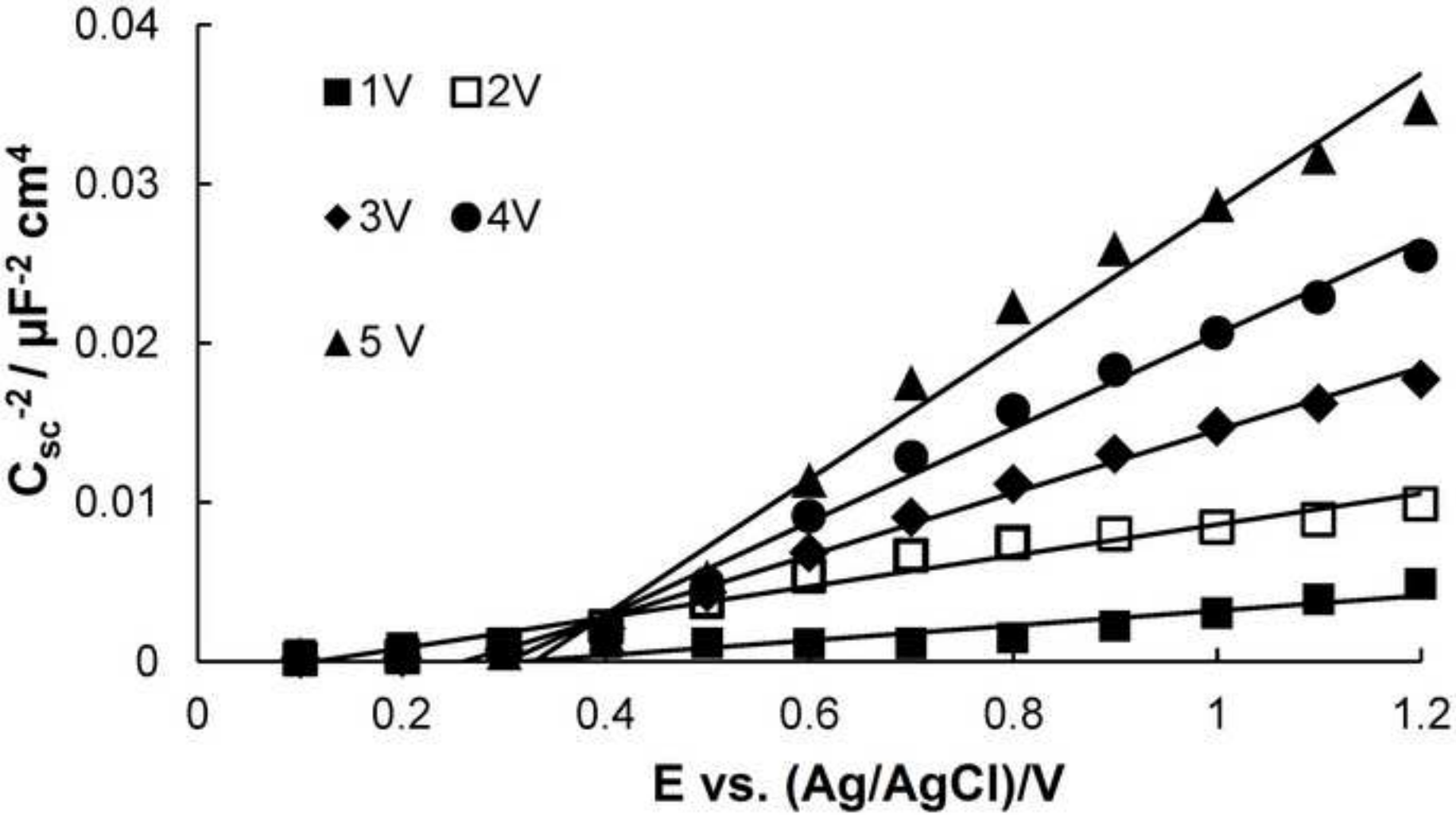
0.04
0.03
0.02
0.01
0
1V
2V
3V
4V
5 V
C_{sc}^{-2} / μF^{-2} cm^4
0
0.2
0.4
0.6
0.8
1
1.2
E vs. (Ag/AgCl)/V

Figure 8

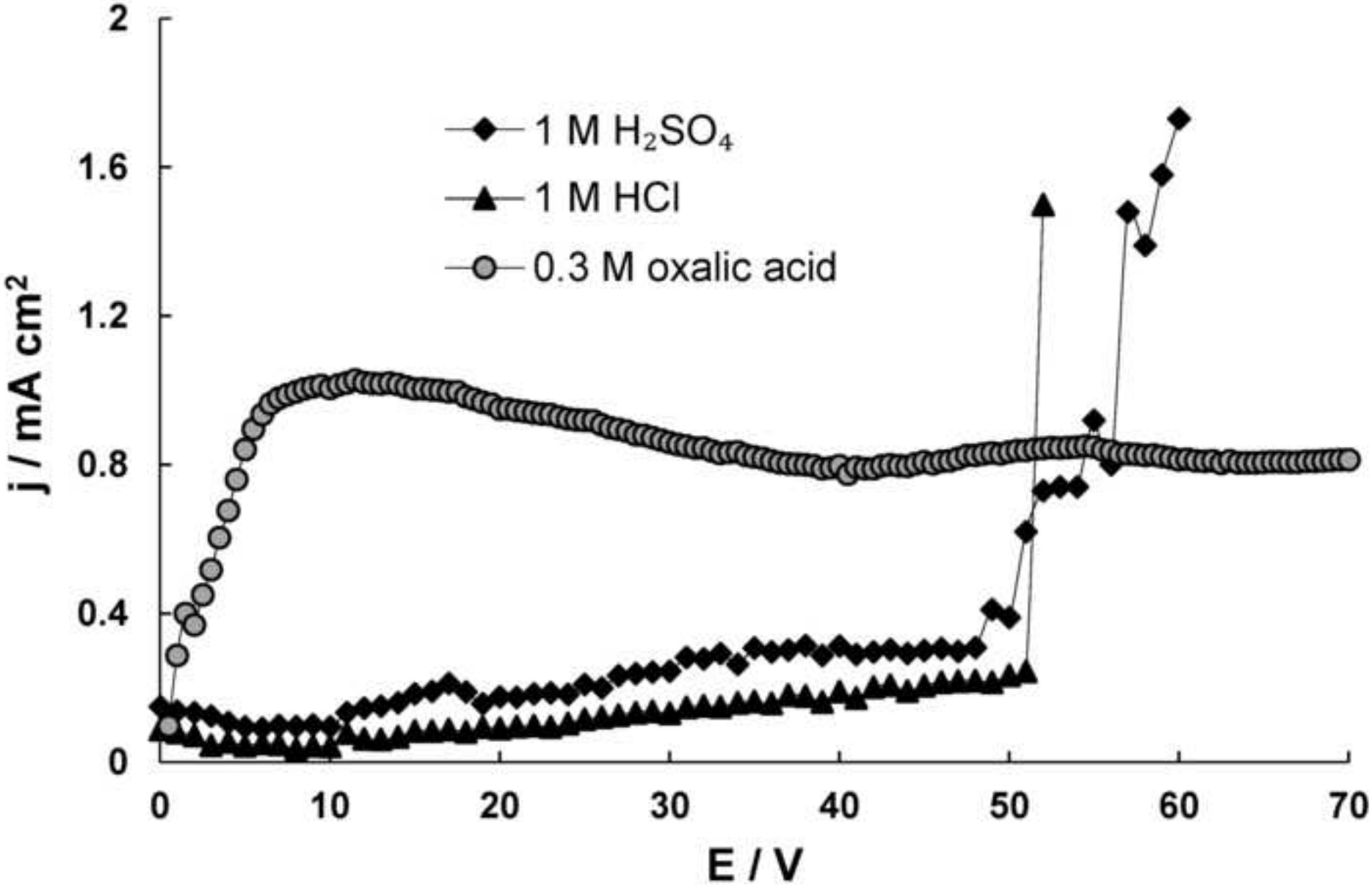
2
1.6
1.2
0.8
0.4
0
j / mA cm^2
1 M H_2SO_4
1 M HCl
0.3 M oxalic acid
0
10
20
30
40
50
60
70
E / V

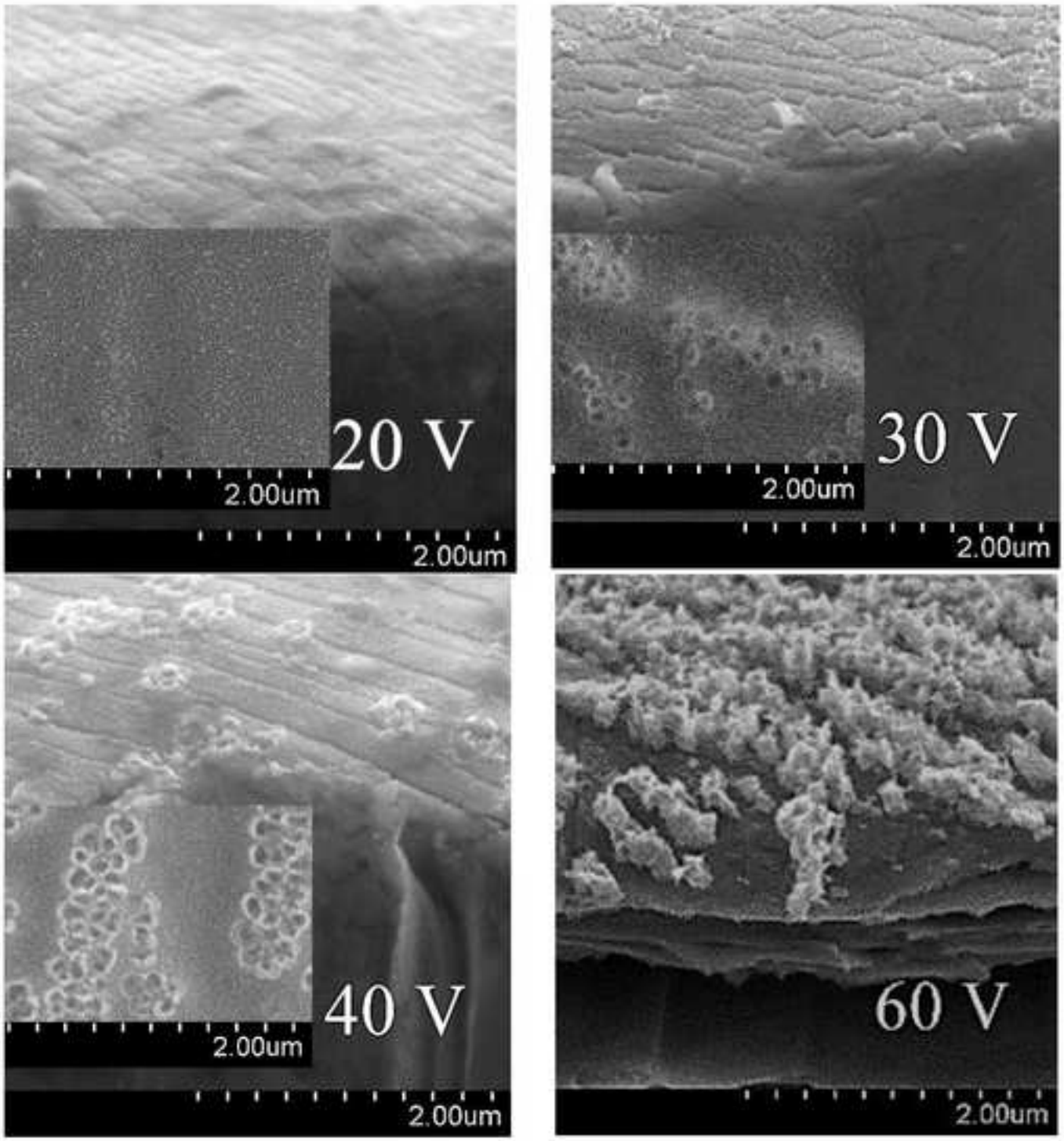

Figure 10

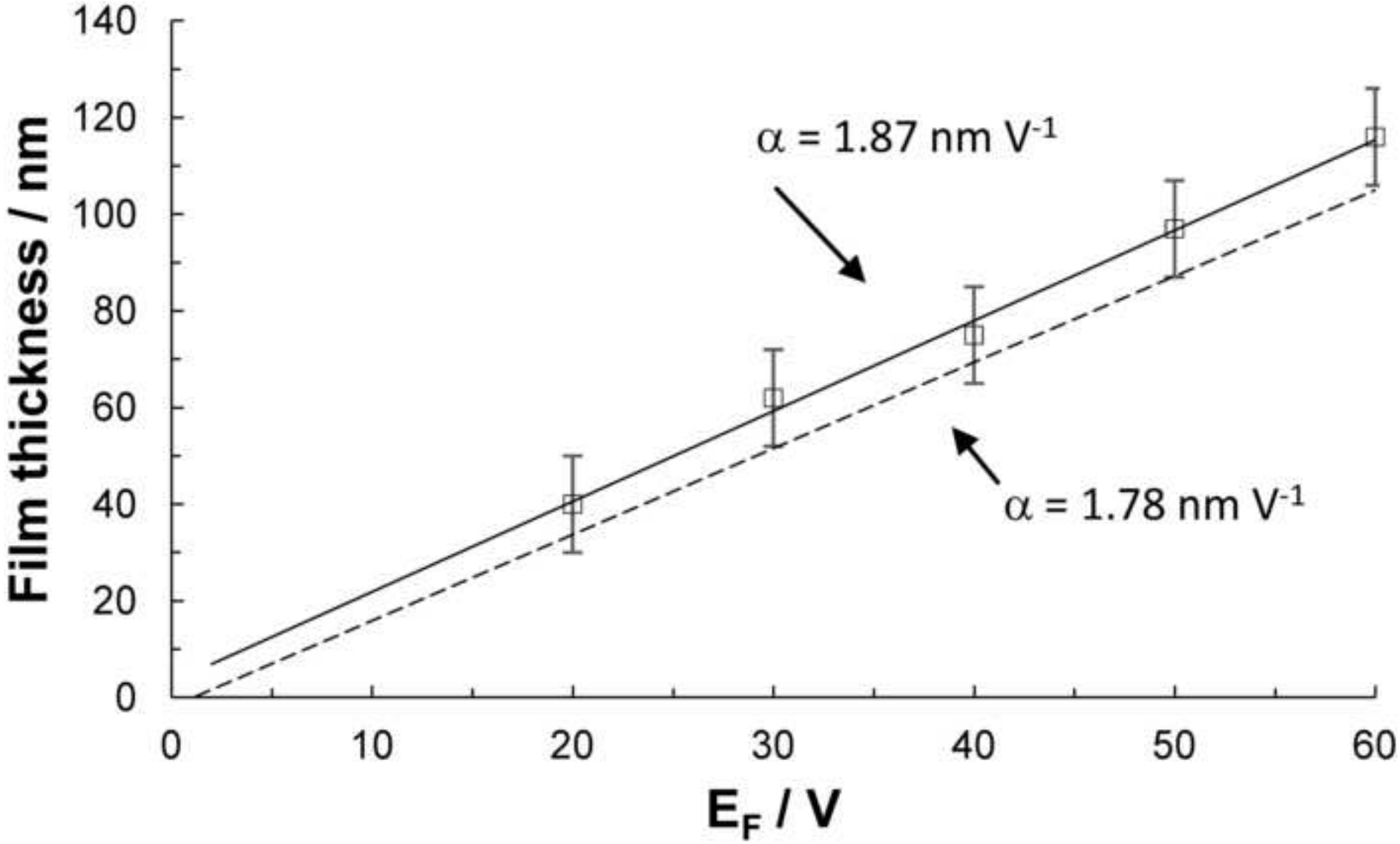
Film thickness / nm
140
120
100
80
60
40
20
0
0
10
20
30
40
50
60
E_F / V
α = 1.87 nm V-1
α = 1.78 nm V-1

Figure 11

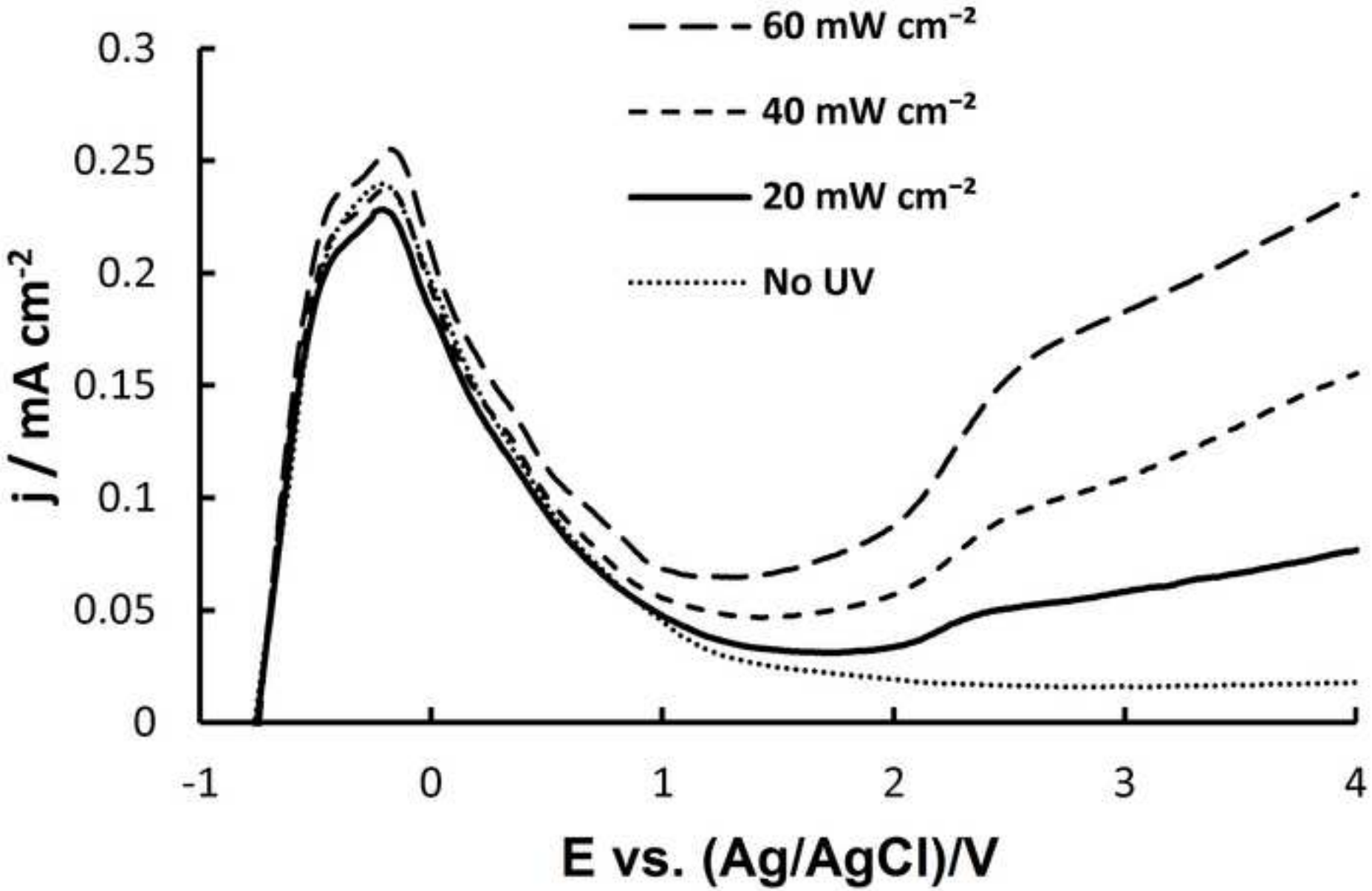
60 mW cm⁻²
40 mW cm⁻²
20 mW cm⁻²
No UV
j / mA cm-2
0.3
0.25
0.2
0.15
0.1
0.05
0
-1
0
1
2
3
4
E vs. (Ag/AgCl)/V

Figure 12

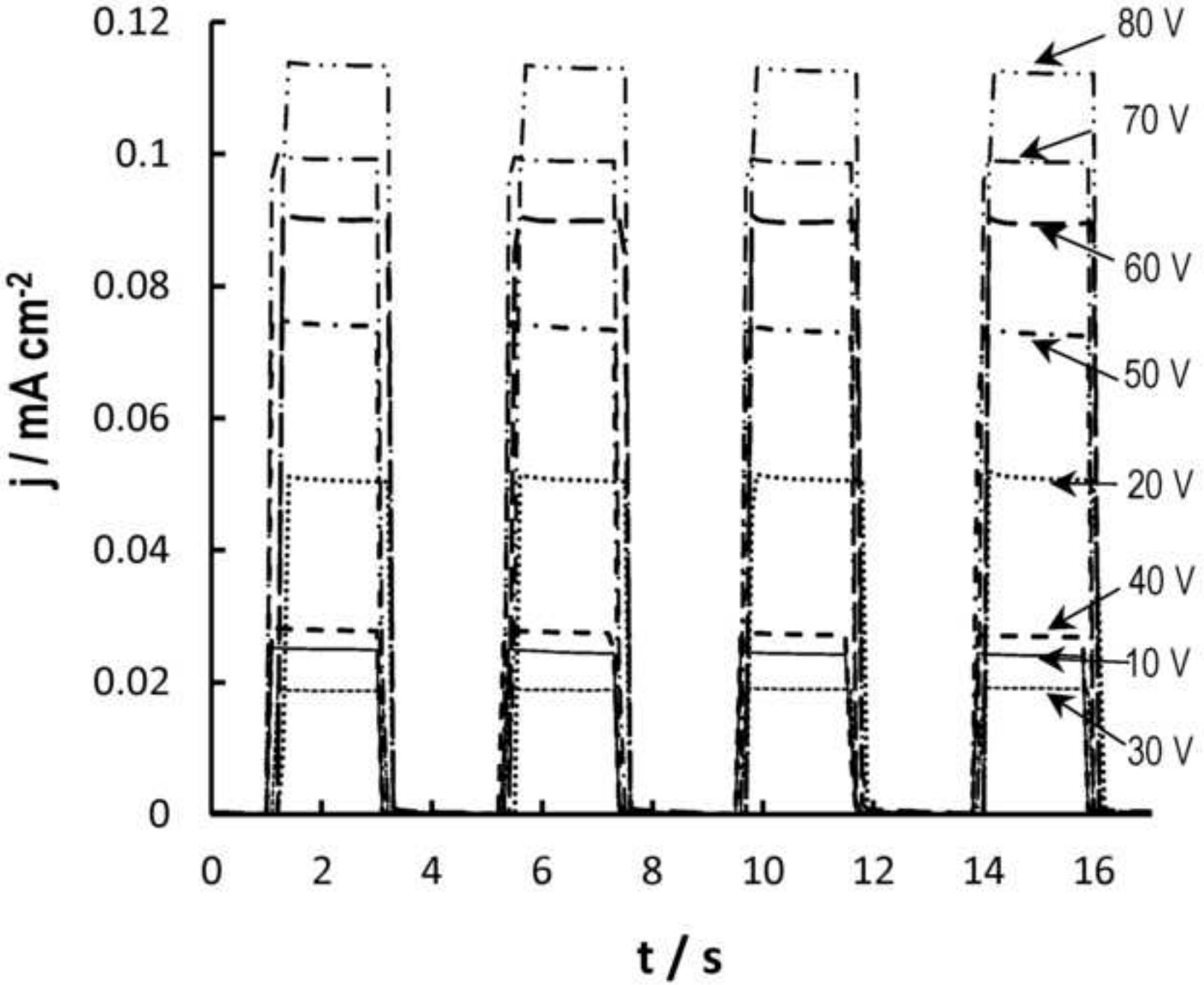
0.12
0.1
0.08
0.06
0.04
0.02
0
j / mA cm-2
0
2
4
6
8
10
12
14
16
t / s
80 V
70 V
60 V
50 V
20 V
40 V
10 V
30 V

Figure 13

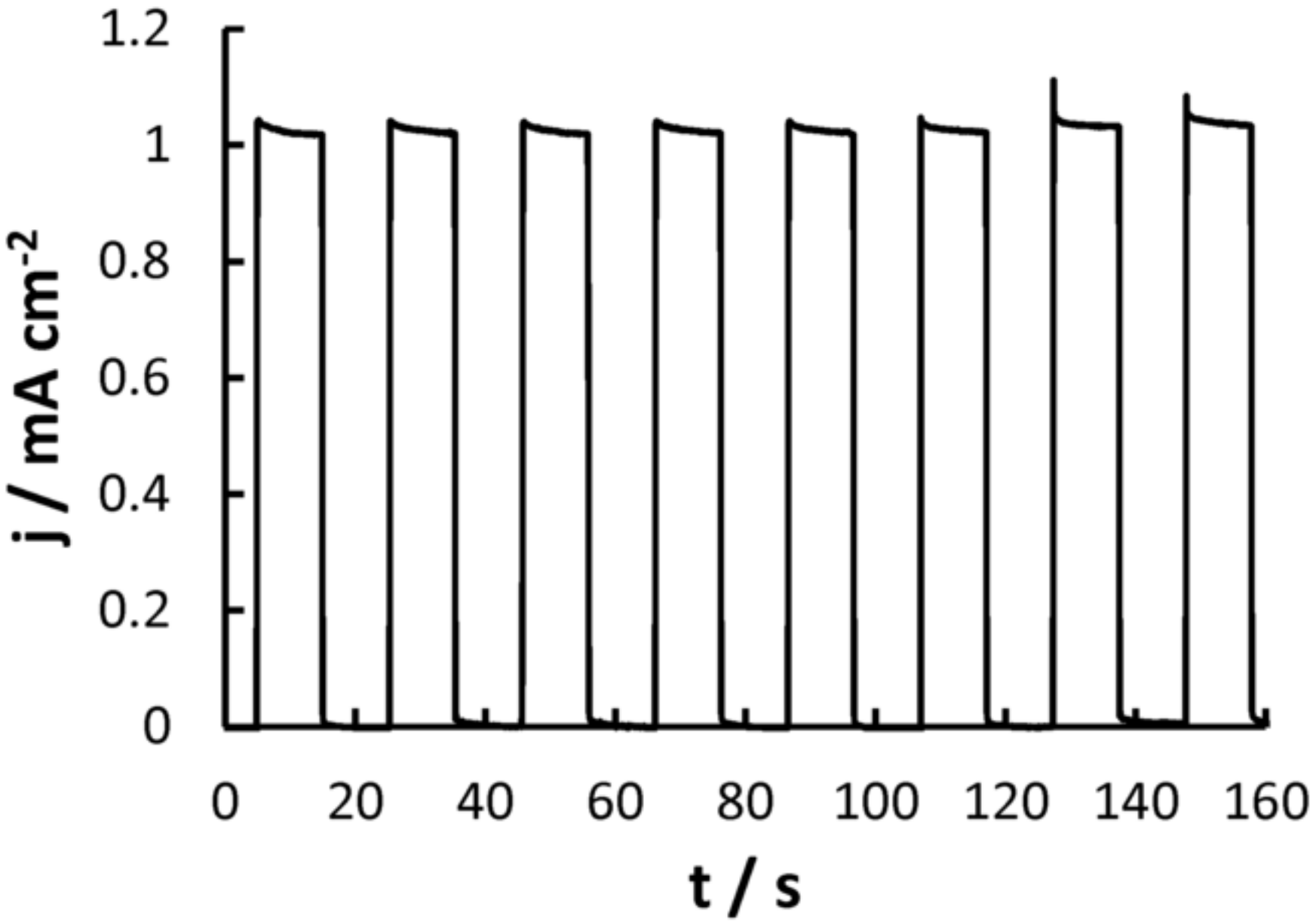

Figure 14